NEAR-INFRARED IMAGING OF WHITE DWARFS WITH CANDIDATE DEBRIS DISKS

Zhongxiang Wang[1], Anestis Tziamtzis[1], and Xuebing Wang[1,2]

[1] Shanghai Astronomical Observatory, Chinese Academy of Sciences, 80 Nandan Road, Shanghai 200030, China
[2] Graduate University of Chinese Academy of Sciences, No. 19A, Yuquan Road, Beijing 100049, China

ABSTRACT

We have carried out JHK_s imaging of 12 white dwarf debris disk candidates from the WIRED Sloan Digital Sky Survey Data Release 7 catalog, aiming to confirm or rule out disks among these sources. On the basis of positional identification and the flux density spectra, we find that seven white dwarfs have excess infrared emission, but mostly at *Wide-field Infrared Survey Explorer W1* and *W2* bands. Four are due to nearby red objects consistent with background galaxies or very low mass dwarfs, and one exhibits excess emission at JHK_s consistent with an unresolved L0 companion at the correct distance. While our photometry is not inconsistent with all seven excesses arising from disks, the stellar properties are distinct from the known population of debris disk white dwarfs, making the possibility questionable. In order to further investigate the nature of these infrared sources, warm *Spitzer* imaging is needed, which may help resolve galaxies from the white dwarfs and provide more accurate flux measurements.

Key words: circumstellar matter – infrared: stars – white dwarfs

Online-only material: color figure

1. INTRODUCTION

The discovery of the first circumstellar debris disk around a white dwarf (WD; G29-28) was made by Zuckerman & Becklin (1987; see also Jura 2003; Reach et al. 2005). Since then, due to the *Spitzer Space Telescope* as well as large survey programs, over 20 WDs have been identified to have debris disks (see, e.g., von Hippel et al. 2007; Farihi et al. 2009; Xu & Jura 2012; Girven et al. 2012 and references therein). It is believed that such a debris disk is formed from material produced by tidal disruption of asteroids within the Roche radius of a WD (Graham et al. 1990; Jura 2003), since planetary material is known to commonly exist around the progenitor stars of WDs and it has been suggested that part of the material can survive through late phases of stellar evolution (e.g., Debes & Sigurdsson 2002).

This picture has been supported by derived properties of several gaseous metal disks around isolated WDs (Gänsicke et al. 2006, 2007, 2008; Melis et al. 2012), detailed infrared studies of the debris-disk WD systems (e.g., Reach et al. 2005, 2009; von Hippel et al. 2007; Jura et al. 2007), and more common detections of absorption features of high-Z metals in WD spectra (Zuckerman et al. 2003; Klein et al. 2011 and references therein). The high-Z spectral features are considered as a result of the processes of asteroids disruption and subsequent WD accretion of high-Z material probably through a disk. The accreted material pollutes the expectedly "pure" hydrogen or helium atmosphere (Jura 2008), since the primordial metals within the atmospheres of WDs sink rapidly (Paquette et al. 1986). Therefore, one important application of the observational studies of the polluted WDs is that it can provide information about bulk elemental compositions of extrasolar planets (see, e.g., Zuckerman et al. 2007; Klein et al. 2011; Gänsicke et al. 2012).

The large survey of WD debris-disk systems is warranted as the resulting increased samples allow detailed studies of disk formation and accretion processes around WDs (Jura 2008; Rafikov 2011) and that of the disk properties and disk-existence frequency indicating the corresponding properties of planetary bodies (Girven et al. 2012; Barber et al. 2012). Recently, the

Data Release 7 (DR7) WD catalog from the Sloan Digital Sky Survey (SDSS), which contains nearly 20,000 sources, was released (Kleinman et al. 2013). Using the infrared all-sky data from the *Wide field Infrared Survey Explorer* (*WISE*), Debes et al. (2011) conducted a thorough search for infrared counterparts to WDs in the DR7 catalog, and found 52 candidate debris disks (we name these sources "dxxxx" in this paper) and 69 candidate counterparts with indeterminate infrared excess emission (which were defined such because both a debris disk and a brown-dwarf companion can explain their excess emission; these sources are named "ixxxx" in this paper). For the first and latter types of the counterparts, there are 32 and 54, respectively, that did not have detections at JHK_s bands (basically in either the Two Micron All Sky Survey (2MASS) or the UKIDSS survey). Since *WISE* imaging had a FWHM of $>6''$ (Wright et al. 2010), source confusion could cause misidentification of excess emission. In order to identify the counterparts among these candidates, and, if identified, to provide more measurements for determining the debris-disk sources, we have carried out ground-based imaging of the candidates that did not have JHK_s flux measurements. In this paper, we report the results from our observations.

2. OBSERVATIONS AND DATA REDUCTION

2.1. Ground-based Imaging

We carried out observations with the 5.1 m Hale telescope at Palomar Observatory in the United States. Through the Chinese Telescope Access Program, we were awarded two nights in 2012 November and two half nights in 2013 February. Unfortunately, only the night of 2012 November 27–28 was clear and useful data were taken. The instrument used was the Wide field IR Camera (WIRC; Wilson et al. 2003), which has a 2048×2048 pixel^2 Hawaii-II HgCdTe detector. The pixel scale was $0''.249$ pixel^{-1} and the field of view was $8'.7$.

For the 86 WDs we chose to observe, we used published results of their effective temperature and optical magnitudes to estimate their lower flux limits at JHK_s bands (Debes et al. 2011; Kleinman et al. 2013; see also Table 1), assuming

Table 1
Properties of 12 WD Targets

Name	u'	g'	r'	i'	z'	T (K)	$\log^a (g)$	$A_{g'}$	d (pc)
i000410.42−034008.6	17.46	16.93	16.76	16.72	16.74	6887	7.71	0.15	51
i011616.95−094347.9	20.09	19.39	19.08	18.97	18.95	6309	8.06	0.16	104
i073018.36+411320.4	17.03	16.61	16.92	17.10	17.38	15126	7.83	0.26	133
i074631.42+173448.2	17.93	17.57	17.59	17.66	17.82	9282	8.59	0.14	66
d081308.52+480642.3	16.30	16.54	16.97	17.30	17.60	32727	7.86	0.20	279
i083633.00+374259.4	19.21	18.71	18.67	18.66	18.73	7798	8.11	0.12	116
i085650.58+275118.0	18.76	18.63	18.92	19.21	19.35	19333	7.86	0.12	428
d090611.00+414114.3	16.73	17.14	17.64	17.97	18.19	47637	7.91	0.05	469
i091312.74+403628.8	18.14	17.64	17.86	18.02	18.25	11726	8.02	0.07	153
i101007.89+615515.7	19.38	18.89	18.73	18.71	18.68	7252	8.31	0.04	94
i102915.97+300251.6	19.42	18.98	18.88	18.97	18.93	7755	7.86	0.08	153
i231725.29−084032.9	18.94	18.38	18.19	18.13	18.14	6862	7.34	0.13	124

Note. [a] $\log(g)$ is in units of cm s^{-2}.

Table 2
Near-infrared and WISE Measurements of 12 WD Targets[a,b]

Name	J Filter		H Filter		K_s Filter		W1	W2	W3	W4
	t_{exp}	J	t_{exp}	H	t_{exp}	K_s				
i000410.42−034008.6	0.27	16.05 ± 0.04	0.27	16.01 ± 0.07	0.27	15.80 ± 0.07	15.40 ± 0.05	15.51 ± 0.2	12.5	8.8
i011616.95−094347.9	5.0	18.38 ± 0.09	5.0	18.05 ± 0.10	5.0	17.86 ± 0.11	17.0 ± 0.2	16.2	12.7	9.1
i073018.36+411320.4	0.83	17.07 ± 0.04	1.7	17.20 ± 0.06	2.5	16.91 ± 0.08	16.3 ± 0.2	16.2	12.7	8.9
073018.20+411320.4[c]		18.44 ± 0.06		18.06 ± 0.08		17.84 ± 0.07				
i074631.42+173448.2	1.3	17.26 ± 0.05	1.7	17.37 ± 0.08	2.5	17.29 ± 0.09	16.5 ± 0.1	16.7 ± 0.5	12.1	8.5
d081308.52+480642.3	1.3	17.50 ± 0.04	2.5	17.60 ± 0.06	5.0	17.47 ± 0.06	16.5 ± 0.1	16.6 ± 0.4	12.8	8.6
081308.61+480643.4[c]		17.82 ± 0.06		17.25 ± 0.05		16.09 ± 0.04				
i083633.00+374259.4	2.5	18.03 ± 0.06	5.0	18.05 ± 0.08	10	17.92 ± 0.13	17.0 ± 0.2	17.0	12.4	8.8
i085650.58+275118.0	7.2	18.27 ± 0.09	16.2	18.30 ± 0.09	27	18.41 ± 0.16	16.8 ± 0.2	16.2	12.5	8.5
d090611.00+414114.3	2.5	18.12 ± 0.05	5.0	18.28 ± 0.07	7.5	18.59 ± 0.09	15.15 ± 0.04	14.71 ± 0.07	12.4	9.4
090611.09+414115.1[c]		18.20 ± 0.05		17.45 ± 0.05		16.44 ± 0.04				
i091312.74+403628.8	2.5	17.97 ± 0.05	2.5	17.95 ± 0.06	5.0	18.10 ± 0.09	17.1 ± 0.2	16.3	12.8	8.7
091312.73+403631.3[c]		19.44 ± 0.16		18.68 ± 0.07		17.92 ± 0.08				
i101007.89+615515.7	2.5	18.09 ± 0.07	5.0	17.95 ± 0.08	5.0	17.68 ± 0.05	16.34 ± 0.07	16.5 ± 0.3	13.2	9.4
i102915.97+300251.6	5.0	18.51 ± 0.06	5.0	17.97 ± 0.10	7.5	18.27 ± 0.10	16.7 ± 0.1	16.1 ± 0.3	12.6	9.1
i231725.29−084032.9	3.3	17.42 ± 0.05	3.3	17.37 ± 0.08	2.5	16.92 ± 0.10	16.5 ± 0.1	16.1	12.4	8.8

Notes.
[a] Exposure time t_{exp} at each band is in units of minute.
[b] For WISE measurements, magnitudes without uncertainties are upper limits.
[c] Nearby stars that are marked as object B in Figure 1, with their names giving the positions measured by our near-infrared imaging.

pure blackbody emission. Based on the estimated flux limits, exposure times at the bands for each target were estimated accordingly. Due to weather limitations, we observed only 12 WDs; the exposure times are given in Table 2. During each exposure, the telescope was dithered in a five-point grid with offsets of ∼40″ to obtain a measurement of the sky background. The observing conditions were mediocre, with the seeing having a median value of 0″.9 but occasionally dropping to 1″.5.

We used IRAF for our data reduction. The images were dark-subtracted and flat-field corrected. In addition, a sky image was made by filtering out stars from each set of the dithered images in one exposure. The sky image was subtracted from the set of images, and then the sky-subtracted images were shifted and combined into one final image of a target field.

To calibrate our target images astrometrically, we used the in-field, relatively bright 2MASS stars (Skrutskie et al. 2006), the numbers of which were between 8 and 50, depending on the fields. The resulting nominal uncertainties of the calibrated images are in a range of 0″.03–0″.11. For most of our images,

the uncertainties are dominated by the 2MASS systematic uncertainty of ≃0″.15 (with respect to the International Celestial Reference System).

We used the IRAF aperture photometry package apphot to measure the brightnesses of our sources for most of the images. For a few cases in which a target was resolved to have a nearby source, the point-spread function fitting package daophot was used. Flux calibration was conducted by comparing to bright 2MASS stars detected in our images.

2.2. WISE Imaging

Launched in 2009 December 14, WISE mapped the entire sky at 3.4, 4.6, 12, and 22 μm (called W1, W2, W3, and W4 bands, respectively) in 2010 with FWHMs of 6″.1, 6″.4, 6″.5, and 12″.0 in the four bands, respectively (see Wright et al. 2010 for details). The WISE all-sky images and source catalog were released in 2012 March. We downloaded the flux measurements of each target in the source catalog and the WISE image data of each
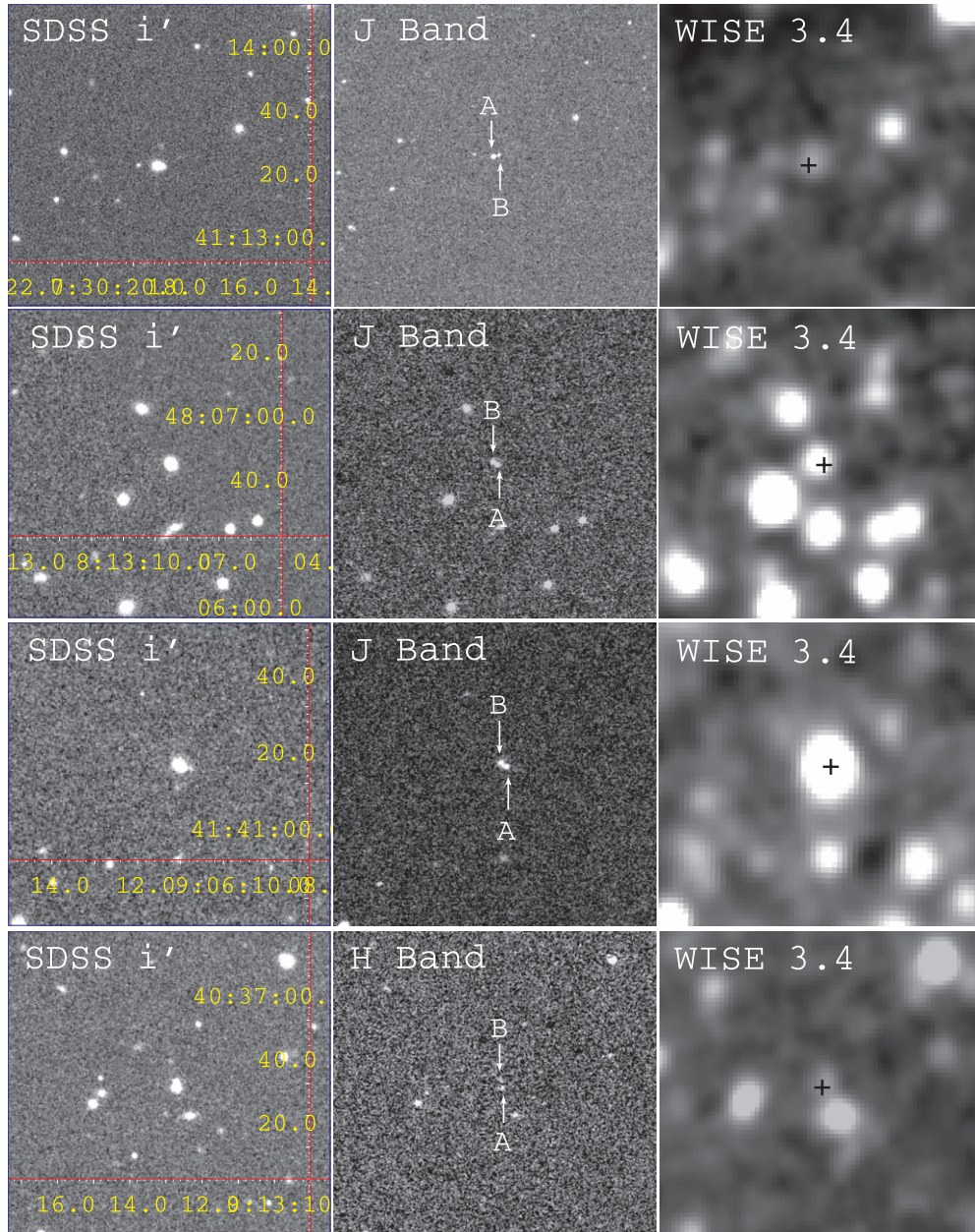
Figure 1. Near-infrared images of WDs i0730, d0813, d0906, and i0913. These four WDs, marked as object *A* in the middle panels, are resolved to have a nearby source (marked as object *B*). The SDSS *i'* (left panels) and *WISE W*1 band (right panels) images are shown for comparison. The SDSS positions of the WDs are marked by plus signs in the *WISE* images.

(A color version of this figure is available in the online journal.)

target field from the Infrared Processing and Analysis Center. Debes et al. (2011) provided all magnitudes or magnitude upper limits of the *WISE* candidate counterparts to the WD targets, but because they used the *WISE* preliminary catalogs, the values were slightly different from those in the all-sky source catalog. We therefore re-provided the magnitudes or magnitude upper limits of our 12 WD targets from the all-sky source catalog in Table 2.

3. RESULTS

3.1. Positional Identification

In our ground-based images, we detected all 12 targets, but we found that 4 of them were resolved as 2 sources at/near the *WISE* source position. The fields of the four WDs are shown in

Figure 1. From our astrometry, we determined the counterparts based on the measured positions and they are marked as object *A* in Figure 1. The nearby non-counterpart sources, which are $1''$–$2''$ away from the counterparts, are marked as object *B*. We also determined the positions and JHK_s magnitudes of these nearby sources, and the values are given next to the counterparts in Table 2. For the other eight targets, one single source was clearly detected at or near the SDSS position. Among them, i0004 was detected by the 2MASS survey, but because it had significant proper motion, $\Delta\alpha = 2''86 \pm 0''06$ and $\Delta\delta = -0''22 \pm 0''04$ (our Palomar measurement with respect to that of 2MASS, which was made on 1998 September 17), it was not reported to have the 2MASS detections (the positional criterion for candidate counterpart identification was $2''0$ in Debes et al. 2011).
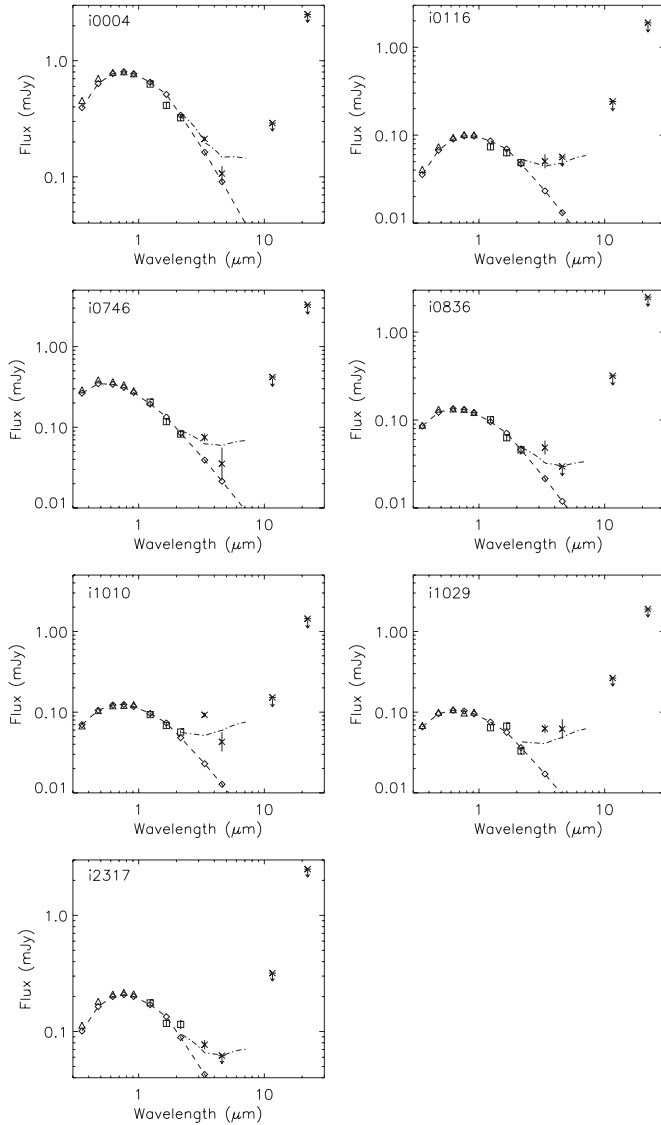
Figure 2. Flux density spectra of seven WDs that possibly have a debris disk. The SDSS optical, our Palomar JHK_s, and *WISE* $W1/W2$ fluxes are displayed as triangles, squares, and crosses, respectively. The *WISE* flux upper limits are also shown. The model fluxes of each WD at the bands are indicated by diamonds and connected by the dashed curve, and the best-fit debris disk model spectrum is plotted as the dash-dotted curve.

3.2. Flux Density Spectra

Combining SDSS $u'g'r'i'z'$ flux measurements (Kleinman et al. 2013) and that from the *WISE* all-sky source catalog with our JHK_s measurements, we constructed the flux density spectra for the 12 WD targets. The spectra are shown in Figures 2 and 3. For the four WDs with a nearby source, the nearby sources are included correspondingly in the figure (displayed as circular data points). We compared our observational spectra with WD model spectra in the infrared bands (kindly provided by P. Bergeron), whose properties were determined by Kleinman et al. (2013; see also Debes et al. 2011), and found that no significant excess emission at JHK_s bands was detected for most of the WDs except i0856. For i0730, d0813, d0906, and i0913, the emission detected by *WISE* more likely came from their nearby source (see Section 4.2 below), and our observations excluded them as the WDs with excess infrared emission.
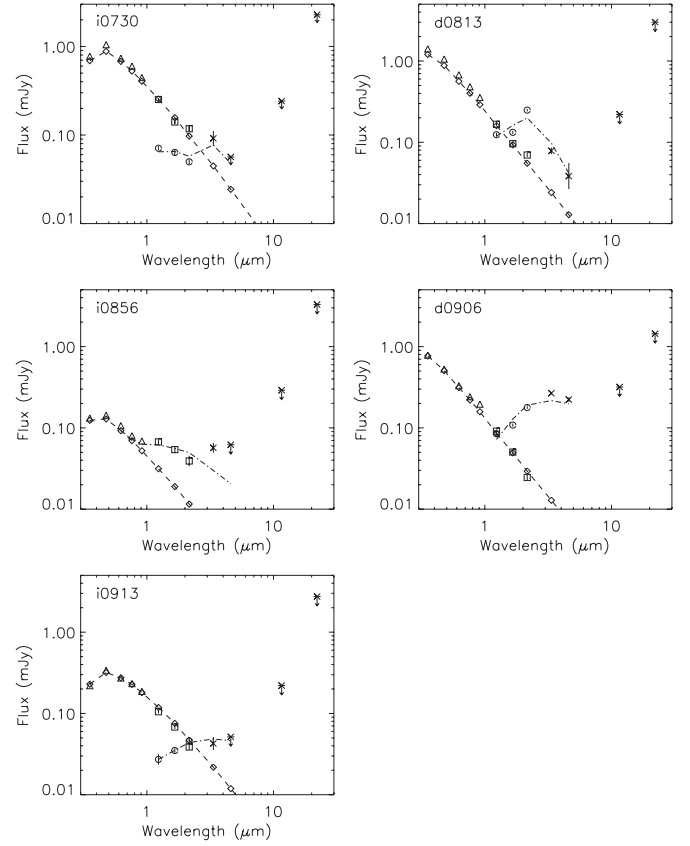

Figure 3. Flux density spectra of five WDs that possibly have either a VLM dwarf nearby in the field or a possible dwarf companion (only for i0856). Symbols are the same as in Figure 2, except with the dash-dotted curve indicating the best-fit brown dwarf model spectrum and the circular data points the fluxes of object *B* in Figure 1.

4. DISCUSSION AND SUMMARY

We observed 12 WDs that were identified to have excess emission from the *WISE* survey by Debes et al. (2011) but did not have previous JHK_s measurements. Given the excess emission, they have been suggested to either have a debris disk or a brown dwarf companion (Debes et al. 2011). From our observations, we found that seven of them did not have significant excess emission at JHK_s bands, while i0856 had strong excess emission, consistent with fluxes measured at the SDSS $r'i'z'$ bands. In addition, four WDs were resolved to have a nearby source. Below including our results, we first discuss the possible origins for the excess emission from the WDs and for the resolved nearby sources, and then provide a summary for the discussion.

4.1. Candidate Debris Disk Sources?

For the seven WDs without significant JHK_s excess emission, they are not likely to have a very low mass (VLM) star or a brown dwarf companion. For example, the K_s magnitudes and their uncertainties are 15–18 and ∼0.1, respectively. The uncertainties only allow the possible existence of 10% excess emission or 2.5 mag fainter sources. Adding 2.5 mag to K_s and comparing it to $W1$ magnitudes, which are slightly lower than K_s values (see Table 2), such infrared sources would have a $K_s - W1$ color of >2.5 mag. The color is too red for VLM dwarfs (see Kirkpatrick et al. 2011 for the colors of the known VLM dwarfs).

Table 3
Results from Debris-disk Fitting

Name	$\cos i$	χ^2/dof
i0004	0.18	7.5/2
i0116	0.93	1.1/1
i0746	0.32	1.5/2
i0836	0.30	7.4/1
i1010	1.0	46/2
i1029	1.0	20/2
i2317	0.46	11/2

With constraints from our JHK_s measurements, we fit these sources with the debris disk model given by Jura (2003) to study if the excess emission could arise from a debris disk. In the model, the disk temperature follows $T(r) \propto T_{\mathrm{WD}} r^{-3/4}$, where T_{WD} is the effective temperature of a WD and r the disk radius (Jura 2003). We adopted the model parameters used in Debes et al. (2011), assuming a temperature of $T = 1200$ K at the inner edge of the debris disk and an outer disk radius of $80 r_{\mathrm{WD}}$, where r_{WD} is the radius of a WD. The distance, effective temperature, and extinction of each WD target were fixed at the values given in Table 1 (Debes et al. 2011; Kleinman et al. 2013). The free parameter was the inclination angle i of the disk. We fit K_s, $W1$, and $W2$ (or only K_s and $W1$ when there was no $W2$ detection) fluxes, where K_s was included to serve as the additional constraint (for i2317, which had K_s excess emission, H-band flux was included as well). We also required that the model flux at $W2$ band must be lower than the *WISE* flux upper limit for the sources not detected at $W2$. We found that the excess emission from most of the sources is generally consistent with arising from a debris disk, and the resulting best-fit $\cos i$ and χ^2 values are summarized in Table 3. The best-fit model fluxes for each source are shown in Figure 2.

For i0836 and i2317, the requirement of the model for the $W2$ flux lower than the *WISE* upper limit provided a constraint in the fitting. If this requirement is not considered, χ^2 values would be much smaller. For i1010 and i1029, the χ^2 values are quite large for $\cos i = 1$. This is because their $W1$ fluxes are significantly higher than their K_s fluxes, and in order for the model to match the $W1$ fluxes, the model fluxes were increased, thus inducing large χ^2 values at K_s band. We note that since the *WISE* magnitudes of the WDs are in a range of 15–17 and *WISE* photometry of such faint sources is known to have as large as ∼0.4 mag systematic uncertainty,[3] the poor fitting can be caused by the large uncertainties on *WISE* photometry that are not included in the catalog data. For the same reason, we did not further search for better fitting by varying the model parameters.

However, for the WDs that show clear excess emission and are believed to have a debris disk, we know that (1) they nearly all have effective temperatures in a range of 9500–24,000 K (except G 166−58 for its $T_{\mathrm{WD}} = 7400$ K; Farihi et al. 2008); (2) they nearly all are known to be metal-rich from optical spectroscopy (Xu & Jura 2012); and (3) nearly half of them show significant emission excesses at infrared K band relative to their WD model spectra. These properties make the identification of the seven WDs as candidates with debris disks highly questionable. The seven WDs generally do not fit in any of them (Tables 1 and 3; Debes et al. 2011).

---

[3] See http://wise2.ipac.caltech.edu/docs/release/allsky/expsup/sec6_3c.html.

4.2. Candidate Brown Dwarf Sources?

Since *WISE* imaging had relatively low spatial resolution, it cannot be determined solely based on the positions whether or not the *WISE* sources are the counterparts to the nearby sources of i0730, d0813, d0906, and i0913 (object B in Figure 1). Combining our JHK_s measurements with the *WISE* fluxes, as shown in Figure 3, the overall broadband spectra suggest that the *WISE* sources are the counterparts to the four nearby sources, or at least emission from the nearby sources dominated over that from the four WDs (otherwise these nearby sources would have to have an unlikely, large flux decrease from K_s to $W1$). Since the sources are red and three of them (nearby to ixxxx sources) were classified by Debes et al. (2011) to be possible candidate brown dwarfs, we fit their broadband spectra with that of VLM stars and brown dwarfs. Following Debes et al. (2011), we used the empirical spectra for M, L, and T dwarfs (Hawley et al. 2002; Kirkpatrick et al. 2011). We first fixed the distances at the values of the WDs and found that the resulting χ^2 were large (the values and the best-fit spectral types are given in Columns 4 and 3, respectively, of Table 4). Setting the distance as a free parameter, the best-fit χ^2 can be significantly reduced (see the values at column seven of Table 4). Therefore, if the sources are M or L dwarfs, as identified from our fitting, they are most likely not associated with the WDs. The best-fit spectra of the four sources are shown in Figure 3.

In addition for i0856, since it had significant excess emission starting from the optical z' to JHK_s bands comparing to the WD model spectrum, the debris-disk model we used, which assumed a low-temperature disk, could not provide a reasonably well fit. We thus tested with the VLM dwarf models and found that an L0 dwarf at the WD's distance of 428 pc can generally describe the excess emission except at the $W1$ band (Figure 3). Here again given the large uncertainties on the *WISE* measurements of faint sources, we considered the fitting was acceptable although the reduced χ^2 is $\simeq 16$ (Table 4).

4.3. Background Galaxies?

The WD targets are located away from the Galactic plane having clean source fields according to the SDSS optical and our JHK_s images. However, it has been shown from *Spitzer* imaging that at $m > 14$ mag in the wavelength range of 3–10 μm, galaxies dominate in such regions (Fazio et al. 2004). For example, as our WD targets have $W1$ magnitudes in a range of 15–17 mag, at its middle value of 16 mag, the *Spitzer* galaxy count at 3.6 μm was $\simeq 2300$ mag^{-1} deg^{-2} (Fazio et al. 2004) or 1.8×10^{-4} mag^{-1} arcsec^{-2}. Considering the $2''$ radius circular region, which was used by Debes et al. (2011) for searching for WD counterparts, there will be a chance of 0.23% to randomly find at least one 16 mag galaxy in such a region. The percentage is low, but there were nearly 18,000 times searches (for 17,955 unique and valid targets; Debes et al. 2011), which would result in 40 randomly detected galaxies. Approximately 300 WDs per mag were detected at $W1 = 16$ mag, but excluding 23% naked WDs (detection of WD photosphere only) and 67% candidate WD plus M dwarf binaries (Debes et al. 2011), the latter we consider rather certain due to their brightnesses and colors, only 30 per mag would be either debris-disk or brown-dwarf companion systems among the candidates. The numbers thus suggest that the detected excess emission is likely caused by unresolved background galaxies due to *WISE*'s relatively low spatial resolution, and those nearby sources are also likely galaxies.

Table 4
Results from VLM Dwarf Fitting

Name	d^a (pc)	Spectral Type	χ^2/dof	d^b (pc)	Spectral Type	χ^2/dof
i0730B	133	L4	170/4	457	M6	9.1/3
d0813B	279	M6	176/4	166	L0	59/3
i0856	428	L0	97/6	…	…	…
d0906B	469	M5	706/4	110	L5	52/3
i0913B	153	L6	28/3	87	L9	0.85/2

Notes.
[a] Distance fixed at that of the corresponding WD.
[b] Obtained distance when it is set as a free parameter.

4.4. Summary

Among the 12 WD targets identified with excess emission from the *WISE* data, our observations and analysis show that 7 are consistent with having a debris disk, but their properties are not in the likely range for the detectable disks on the basis of the currently known debris-disk WDs. Among the other five WD targets, four are found that their excess emission is caused by the existence of a nearby red source and the remaining one, i0856, shows significant excess emission at JHK_s bands. Our analysis suggests that the nearby sources are possibly unassociated VLM stars or brown dwarfs while excess emission from i0856 is suggestive of an L0 dwarf. However, we also realize that the excess emission (and the nearby sources) might well be caused by background galaxies, which are known to be the dominant, relatively faint sources at wavelengths between 3–10 μm. Therefore, in order to investigate the true nature of the observed excess emission or nearby sources, imaging with *Spitzer* is needed. The *Spitzer* observations will possibly resolve background galaxies from the WD targets and provide accurate flux measurements at the infrared wavelengths of $W1$ and $W2$ bands, both helping identify the debris disks and VLM dwarfs.

REFERENCES

Barber, S. D., Patterson, A. J., Kilic, M., et al. 2012, ApJ, 760, 26
Debes, J. H., Hoard, D. W., Wachter, S., Leisawitz, D. T., & Cohen, M. 2011, ApJS, 197, 38
Debes, J. H., & Sigurdsson, S. 2002, ApJ, 572, 556
Farihi, J., Jura, M., & Zuckerman, B. 2009, ApJ, 694, 805
Farihi, J., Zuckerman, B., & Becklin, E. E. 2008, ApJ, 674, 431
Fazio, G. G., Ashby, M. L. N., Barmby, P., et al. 2004, ApJS, 154, 39
Gänsicke, B. T., Koester, D., Farihi, J., et al. 2012, MNRAS, 424, 333
Gänsicke, B. T., Koester, D., Marsh, T. R., Rebassa-Mansergas, A., & Southworth, J. 2008, MNRAS, 391, L103
Gänsicke, B. T., Marsh, T. R., & Southworth, J. 2007, MNRAS, 380, L35
Gänsicke, B. T., Marsh, T. R., Southworth, J., & Rebassa-Mansergas, A. 2006, Sci, 314, 1908
Girven, J., Brinkworth, C. S., Farihi, J., et al. 2012, ApJ, 749, 154
Graham, J. R., Matthews, K., Neugebauer, G., & Soifer, B. T. 1990, ApJ, 357, 216
Hawley, S. L., Covey, K. R., Knapp, G. R., et al. 2002, AJ, 123, 3409
Jura, M. 2003, ApJL, 584, L91
Jura, M. 2008, AJ, 135, 1785
Jura, M., Farihi, J., Zuckerman, B., & Becklin, E. E. 2007, AJ, 133, 1927
Kirkpatrick, J. D., Cushing, M. C., Gelino, C. R., et al. 2011, ApJS, 197, 19
Klein, B., Jura, M., Koester, D., & Zuckerman, B. 2011, ApJ, 741, 64
Kleinman, S. J., Kepler, S. O., Koester, D., et al. 2013, ApJS, 204, 5
Melis, C., Dufour, P., Farihi, J., et al. 2012, ApJL, 751, L4
Paquette, C., Pelletier, C., Fontaine, G., & Michaud, G. 1986, ApJS, 61, 197
Rafikov, R. R. 2011, ApJL, 732, L3
Reach, W. T., Kuchner, M. J., von Hippel, T., et al. 2005, ApJL, 635, L161
Reach, W. T., Lisse, C., von Hippel, T., & Mullally, F. 2009, ApJ, 693, 697
Skrutskie, M. F., Cutri, R. M., Stiening, R., et al. 2006, AJ, 131, 1163
von Hippel, T., Kuchner, M. J., Kilic, M., Mullally, F., & Reach, W. T. 2007, ApJ, 662, 544
Wilson, J. C., Eikenberry, S. S., Henderson, C. P., et al. 2003, in Proc. SPIE, 4841, 451
Wright, E. L., Eisenhardt, P. R. M., Mainzer, A. K., et al. 2010, AJ, 140, 1868
Xu, S., & Jura, M. 2012, ApJ, 745, 88
Zuckerman, B., & Becklin, E. E. 1987, Natur, 330, 138
Zuckerman, B., Koester, D., Melis, C., Hansen, B. M., & Jura, M. 2007, ApJ, 671, 872
Zuckerman, B., Koester, D., Reid, I. N., & Hünsch, M. 2003, ApJ, 596, 477